

A Numerical Study on Magnetic and Structural Properties of Ni-Doped ZnO Nanoparticles at Extremely Low Temperatures

Adeleh Mokhles Gerami¹ · Mehdi Vaez-Zadeh¹

Received: 22 October 2015 / Accepted: 19 January 2016 / Published online: 29 January 2016
© Springer Science+Business Media New York 2016

Abstract The magnetic properties of Ni-doped ZnO nanoparticles are investigated using a numerical model based on simultaneous solution of the localized partition function and the master equation of particle moment dynamics. In this model, field-cooled and zero field-cooled (FC/ZFC) magnetization and the hysteresis loop are calculated. To provide an accurate model that matches the experimental results, the effect of factors such as nanoparticle distribution and randomly distributed easy axis are considered. The electronic and structural properties of $Zn_{1-x}Ni_xO$ ($x = 0.028, 0.062, \text{ and } 0.125$) are investigated using first-principle calculations within the framework of density function theory. The results of both models show that the Ni-doped ZnO nanoparticles behave ferromagnetically at extremely low temperatures.

Keywords Dilute magnetic semiconductor · FC/ZFC magnetization · Hysteresis loop · Density function theory (DFT) · Ferromagnetism

1 Introduction

ZnO is becoming a topic of increasing interest in studies related to semiconductor materials because of its interesting

electrical, piezoelectric, and optical properties. This material is a promising candidate for fabrication of electrical devices such as light-emitting diodes, sensors, solar cells, and for photo-luminescent applications [1–4]. Recent experimental researches reveal the possibility of improving the electrical behavior of ZnO and further magnetic applications by doping transition metals inside a host semiconductor lattice [5–8]. Examples of industrial applications can be found in the literature and include high-density magnetic data storage disks, magneto-optical devices, and biomedical applications as contrast agents for MRI imaging [9–11]. Of the metal-doped ZnO compounds, a number of experimental researches have been dedicated to Ni-doped ZnO [12–17]. Results have shown that this compound shows great potential for increasing the photocatalyst activity of Ni-ZnO based on Ni concentration [12], and by decreasing the width of the band gap of ZnO, which noticeably improves the magneto-optical effect [16, 17].

In addition to experimental investigations, theoretical and numerical analysis of Ni-ZnO can also provide complete knowledge of the physics of this dilute magnetic semiconductor [18–20], and valuable information about its structural properties [21, 22]. A numerical approach can be used to calculate parameters that have significant effects on the physical properties of the materials under study to determine the optimal experimental conditions.

The present study investigates the physical properties of Ni-ZnO nanoparticles. The calculations are organized in two sections. First, the effect of factors such as temperature, external magnetic field, and volume distribution of nanoparticles on the magnetic properties of a randomly-oriented ensemble of Ni-ZnO nanoparticles is investigated by employing a comprehensive numerical model. This model is based on simultaneous calculation of the localized partition function and the master equation to calculate the

✉ Mehdi Vaez-Zadeh
mehdi@kntu.ac.ir

Adeleh Mokhles Gerami
mokhles_gerami@mail.kntu.ac.ir

¹ Department of Physics, K.N. Toosi University of Technology, Tehran, P.O. Box 15875-4416, Iran

field-cooled and zero-field-cooled (FC/ZFC) magnetization of Ni-ZnO nanoparticles and hysteresis loop magnetization of the assembly where the external magnetic field sweeps from -7 to 7 kOe. The results are compared with available experimental data. These results provide complete information about magnetic characteristics of the assembly such as blocking temperature, remanence, coercive field, and irreversible temperature.

Next, the electronic characteristics of the structure caused by the presence of a Ni atom inside the ZnO host matrix is investigated using density functional theory (DFT) employed in WIEN2k package. The experimental results reported at room temperature [14, 23, 24] indicate that the structure of the ZnO can be considered to be wurtzite. The effect of different Ni concentrations on the structural and magnetic properties of $\text{Zn}_{1-x}\text{Ni}_x\text{O}$ are also studied.

2 Theory

FC/ZFC magnetization and hysteresis loop is first calculated using the partition function and master equation. Next, the results of calculation of the electronic characteristics of the structure caused by the presence of a Ni atom inside the ZnO host matrix are investigated using the generalized gradient approximation (GGA) in the DFT.

2.1 Numerical Magnetic Calculations

Consider a single spherical nanoparticle with volume (V) where its easy axis is aligned along the Z axis. The magnetic moment of this nanoparticle is oriented with polar and azimuthal angles of θ and ϕ with respect to the easy axis. An external magnetic field is applied in the X - Z plane inclined at angle of γ to the easy axis. Because of the existence of easy axis for each nanoparticle, the magnetic moment prefers to align in the easy axis direction. In the absence of an applied magnetic field, the anisotropic energy of the nanoparticle is calculated as $E = KV \sin^2 \theta$, where K is the anisotropy constant. In this relation, two energy minima ($\theta = 0$ and $\theta = \pi$) represent the stable points for which the magnetic moment tends to align itself in their direction. By switching on the external magnetic field, the energy relation includes an additional term as [20]:

$$E = KV \sin^2 \theta - M_s V H (\sin(\theta) \sin(\phi) \sin(\gamma) - \cos(\theta) \cos(\gamma)) \quad (1)$$

where M_s is saturation magnetization and H is the external magnetic field strength. Figure 1 is a schematic of the response of nanoparticles magnetic moments to the external magnetic field.

Figure 1a shows the anisotropic energy of three magnetic fields that are perpendicular to the easy axis. As the

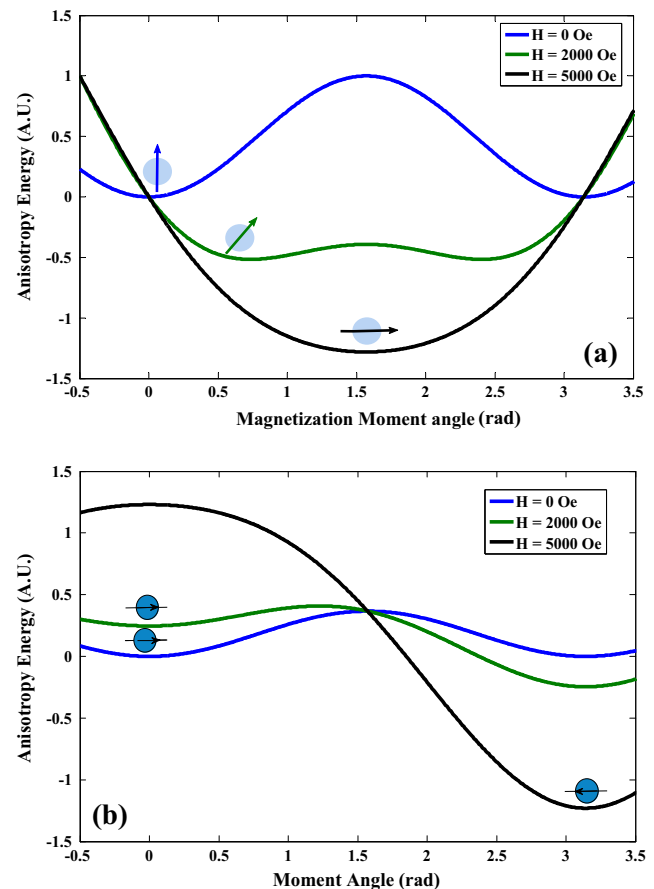


Fig. 1 The response of nanoparticle magnetic moments to the external magnetic field where magnetic field is: **a** Perpendicular to the easy axis. The energy minima moves toward magnetic field direction as magnetic field strength increases. **b** Parallel to the easy axis. Here, the energy minima location does not change in lower fields

magnetic field strength increases, the energy minima shifts toward $\pi/2$ and the energy barrier height decreases. For strengths above the threshold of $H_c = 2K/M_s H \cos(\theta)$, the barrier disappears and a single energy valley with a minimum located at $\pi/2$ remains.

It is worthwhile to study the response of the magnetic moment to the external magnetic fields parallel to the nanoparticle easy axis (Fig. 1b). The magnetic moment of the nanoparticle can initially be oriented in either the parallel or anti-parallel direction with respect to the external magnetic field. As the magnetic field strength increases, the stable points remain in the same place and the barrier height decreases in one direction. Consequently, the magnetic moment of the nanoparticle remains in its initial orientation. Similar to the case shown in Fig. 1a, as the strength of the magnetic field increases to more than the threshold H_c , one of the stable points disappears and the nanoparticle magnetic moment immediately jumps to another stable point. It can be concluded that the orientation of the easy axis with respect to the external magnetic

field plays an important role in calculations related to these magnetic properties.

Thermal fluctuations are other parameters that cause magnetic moment flips between energy valleys which are essential to overcome the energy barrier for low-strength magnetic fields. The mean time between two successive flips is described by Arrhenius law as [25, 26]:

$$\tau_n = \tau_0 \exp\left(\frac{E(H, \theta, \gamma)}{k_b T}\right) \tag{2}$$

where τ_0 , k_b , and T denote the inverse of the attempted frequency, the Boltzmann constant, and the temperature, respectively.

As stated, the particle moments initially occupy one of the stable points. The probability of occupying the i th energy stable valley, P_i , depends on the temperature, barrier height, and relative orientation of the external magnetic field with respect to the easy axis. Additionally, the magnetic moment flips to the alternative direction with rates of τ_1^{-1} and τ_2^{-1} . These probabilities evolve if the temperature (FC/ZFC) or magnetic field (hysteresis loop) changes over time [20, 27]. The probability variation can be described using the master equation for a two level-valley system as:

$$\frac{\partial P(t)}{\partial t} = \frac{P_2}{\tau_2} - \frac{P_1}{\tau_1} \tag{3}$$

which yields:

$$P_i(t) = P_i(0) \exp\left(\frac{-t}{\tau}\right) + \frac{\tau^{-1} - \tau_i^{-1}}{\tau^{-1}} \left[1 - \exp\left(\frac{-t}{\tau}\right)\right] \tag{4}$$

where $\tau^{-1} = \tau_2^{-1} - \tau_1^{-1}$.

This equation can be solved numerically in three modes: FC magnetization, ZFC magnetization, and hysteresis loop. The initial probabilities for each mode can be obtained by assuming that measurement starts at a sufficiently high or low temperature so that the thermal fluctuations are stronger than the barrier height and the particle moment relaxation time is smaller than the measurement time. This means that both the initial P_1 and P_2 probabilities equal 0.5.

In FC magnetization calculations, the sample is subjected to a constant magnetic field and is gradually cooled from a sufficiently high temperature at which all nanoparticles are paramagnetic. In the present model, the probability coefficients are initially set to 0.5 and their evolution is iteratively calculated for each ΔT using (4) by assuming that ΔT decreases by 1 K. For ZFC, the sample is cooled to an extremely low temperature in the absence of the magnetic field. Consequently, $P_1 = P_2 = 0.5$, and ΔT increases by 1 K from the initial low temperature. For the hysteresis loop, the response of the particle moment to a

time-dependent magnetic field is calculated at a constant temperature. In this case, the initial probability is considered to be 0.5 for the initial magnetic field ($H = 0$) because of the random distribution of the magnetic moments for nanoparticles. Considering the effect of random anisotropy axis distribution for all magnetic nanoparticles embedded inside the semiconductor is vital to reach acceptable agreement between the numerical and experimental results.

Depending on the magnitude and orientation of the applied magnetic field, anisotropic energy has either one or two stable points. The particle moment flips very quickly between two stable points in comparison with the time of the relaxation process. For both cases, it can be assumed that the mean localized magnetization is solvable using a localized partition function. If no barrier exists (one stable point), the partition function is defined as [20]:

$$Z_0 = \frac{1}{4\pi} \int_0^{2\pi} \int_0^\pi e^{-\beta E} \sin(\theta) d\theta d\varphi \tag{5}$$

where β is $1/k_B T$. For two stable points, the partition function for the different energy valleys is:

$$\begin{cases} Z_1 = \frac{1}{4\pi} \int_0^{\theta_b} \int_0^\pi e^{-\beta E} \sin(\theta) d\theta d\varphi \\ Z_2 = \frac{1}{4\pi} \int_{\theta_b}^{2\pi} \int_0^\pi e^{-\beta E} \sin(\theta) d\theta d\varphi \end{cases} \tag{6}$$

Therefore, the mean magnetization along the applied field is:

$$M_i(\gamma) = \frac{1}{\beta} \frac{\partial \ln Z_i}{\partial H} \tag{7}$$

In addition to localized magnetization, total magnetization depends on the moment transition rate inward and outwards of the current valley, leading to a change in the probability of valley occupation. The final magnetization, thus, is:

$$M(\gamma) = \sum_{i=0}^2 M_i(\gamma) P_i(H, \gamma, t) \tag{8}$$

For a single energy valley, M_1 and M_2 are zero and the probability of occupation $P_0(H, \gamma, t)$ is always 1. For two energy valleys, M_1 is zero and probabilities $P_1(H, \gamma, t)$ and $P_2(H, \gamma, t)$ evolve over time. The effect of different randomly distributed anisotropies for a particle with volume V can be taken into account by integration of $M_i(\gamma)$ over the whole γ angle as:

$$M^v = \frac{1}{2} \int_0^\pi M_i(\gamma) \sin(\gamma) d\gamma \tag{9}$$

Because real nanoparticles are not exactly the same and their volumes are usually distributed over a log-normal function, the approximation for considering identical volumes can cause deviation from the experimental results. To consider this effect, particle distribution $f(V)$ is used to numerically calculate the magnetization as:

$$M_{tot} = \int_{V_1}^{V_2} M^v f(V) dV \quad (10)$$

In the magnetic simulation of the $Zn_{1-x}Ni_xO$ compound, the nanoparticles are considered to be distributed over a log-normal function with a median diameter of $\langle D \rangle = 2.4$ nm and $\sigma = 0.2$. These values were taken from [15], which reports on the TEM image of Ni nanoparticles doped ZnO single crystal. Moreover, saturation magnetization (M_s) and anisotropic constant (K) are chosen as 40 joule/Oem³ and 1.45×10^5 joule/m³, respectively.

2.2 First Principle Calculation

Using WIEN2k code [28], the structural and magnetic properties of the $Zn_{1-x}Ni_xO$ compound ($x = 0.031, 0.062, \text{ and } 0.125$) is investigated using the first-principle full-potential linearized augmented plane wave method (FP-LAPW) [29] based on DFT. The exchange and correction effects were taken into account by GGA as parameterized by Pedrew et al. [30]. It was experimentally found that the $Zn_{0.97}Ni_{0.03}O$ nanoparticles have a wurtzite hexagonal crystalline structure [31]; however, studies published for other Ni concentrations have reported similar results [14, 23, 24]. Therefore, the wurtzite structure of ZnO is generated with the p63mc space group in the present calculations.

To create a $Zn_{1-x}Ni_xO$ compound with Ni concentrations of 12.5, 6.2, and 2.8 %, $2 \times 2 \times 1$, $2 \times 2 \times 2$, and $3 \times 3 \times 2$ unit cells are considered, respectively (Fig. 2).

Table 1 presents the optimized lattice parameters used. As seen, the optimized lattice constants have been compressed in comparison with the experimental lattice constants of pure ZnO. This can be explained by the ionic radii: the ionic radius of the Ni^{2+} atoms (0.068 nm) is smaller than that of Zn^{2+} (0.074 nm).

In the calculations carried out, cutoff parameter $R_{MT} \times K_{max} = 8.0$, which controls the size of the basis set, was taken into account where R_{MT} is the smallest muffin-tin sphere radius and K_{max} is the maximum value of the reciprocal lattice vectors used in the plan wave expansion. Here, the radius of muffin-tin atomic spheres of Zn, O, and Ni were set to 2.00, 1.72, and 1.96 a.u., respectively, and meshes of $(6 \times 6 \times 6)$, $(6 \times 6 \times 3)$, $(4 \times 4 \times 3)$ k-points in the irreducible part of first Brillouin zone were applied to

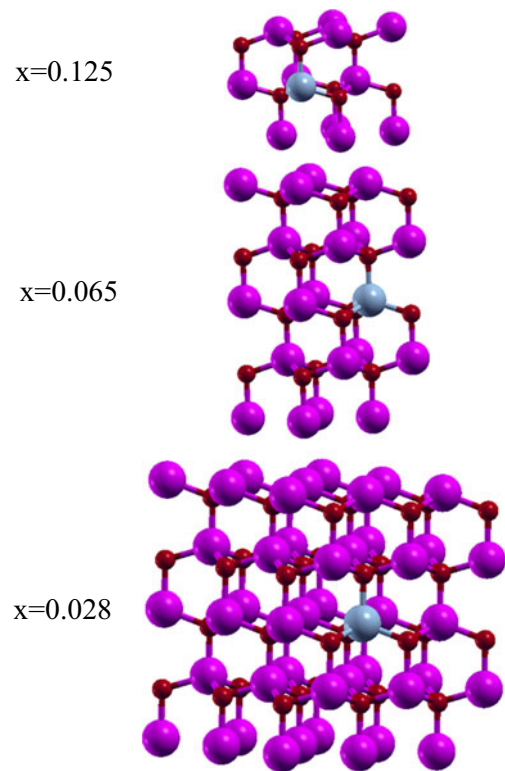


Fig. 2 The crystalline structure of alloys $Zn_{1-x}Ni_xO$ for $x = (0.125, 0.062, \text{ and } 0.028)$. Light blue, violet, and dark red spheres are representative for Ni, Zn, and O, respectively

the self-consistent total energy calculation for the $2 \times 2 \times 1$, $2 \times 2 \times 2$, and $3 \times 3 \times 2$ unit cells, respectively.

3 Results and Discussion

3.1 FC/ZFC Magnetization and Hysteresis Loop Results

The magnetization properties of magnetic nanoparticles are influenced by particle volume distribution, saturation magnetization, and randomly distributed easy axis. In this section, the results of the present numerical model based on solution of the master equation of two energy minima, and a

Table 1 The lattice parameters (a and c) is obtained for different concentration of Ni in ZnO after geometry optimization

Composition	a(nm)	c(nm)	c/a
ZnO ^a	0.325	0.522	1.602
Zn _{0.875} Ni _{0.125} O	0.324	0.521	1.605
Zn _{0.938} Ni _{0.062} O	0.324	0.520	1.604
Zn _{0.972} Ni _{0.028} O	0.324	0.520	1.604

^aExperimental reports [32]

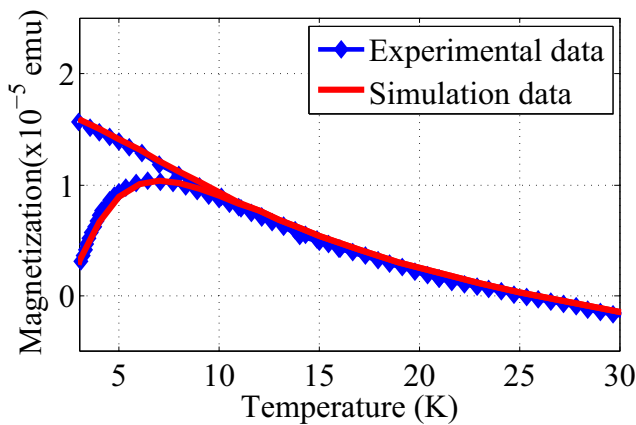


Fig. 3 The comparison of simulated FC/ZFC magnetization of Ni-ZnO with experimental results [15]. The simulation output is in full agreement with the experiment

localized partition function for Ni-doped ZnO nanoparticles are discussed.

The results corresponding to the FC/ZFC magnetization, and hysteresis loop calculations based on the numerical model developed for non-uniform particle distribution have been shown in Figs. 3 and 5, respectively. In Fig. 3, the calculated results are compared with the experimental data reported by Borges et al. [15]. As seen, a peak temperature and irreversibility temperature T_{irr} (temperature at which thermal fluctuation overcomes the barrier height for all nanoparticles) have been obtained around 7 and 12 K, respectively. The results are in good agreement with the experimentally measured data [15].

The blocking temperature (T_B) is the other characteristic of magnetic fine nanoparticles, and is the temperature at which both the magnetic relaxation time of the nanoparticles and the measurement time are the same [33]. For single-volume particles, T_B and the peak temperature of the ZFC

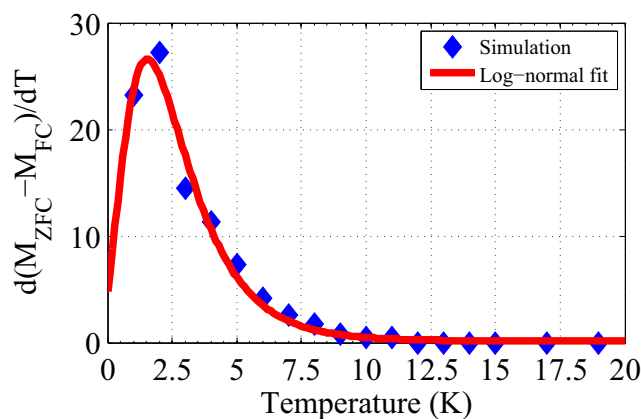


Fig. 4 The Blocking temperature distribution is obtained by log-normal fitting of $d(M_{ZFC} - M_{FC})/dT$. In our case, the average blocking temperature of Ni-ZnO nanoparticles is around 1.6 K

curve coincide. For an ensemble of non-uniform nanoparticles, it can be shown that T_B is distributed over a log-normal function as follows:

$$f(T_B) = \frac{1}{\sqrt{2\pi}\sigma T_B} \exp \left[- \left[\frac{\ln(T_B/\langle T_B \rangle)}{\sqrt{2}\sigma} \right]^2 \right] \quad (11)$$

where $\langle T_B \rangle$ and σ are the median blocking temperature and the width of the distribution function, respectively. Because $d(M_{FC} - M_{ZFC})/dT$ is proportional to the T_B distribution [34], one can derive $\langle T_B \rangle$ and σ by fitting the calculated values for $d(M_{FC} - M_{ZFC})/dT$ into (11) (Fig. 4).

The hysteresis loop is an alternative method which can be used to determine the ferromagnetic and paramagnetic behavior of assembly. In the present study, the hysteresis loop is calculated for temperatures above and below T_{irr} . The calculated hysteresis loops for arbitrarily chosen temperatures are shown in Fig. 5. For $T \leq 10$ K, the relaxation time of the largest nickel nanoparticles become equal to the measurement time ($\tau_m = 100$ s) and ferromagnetic behavior

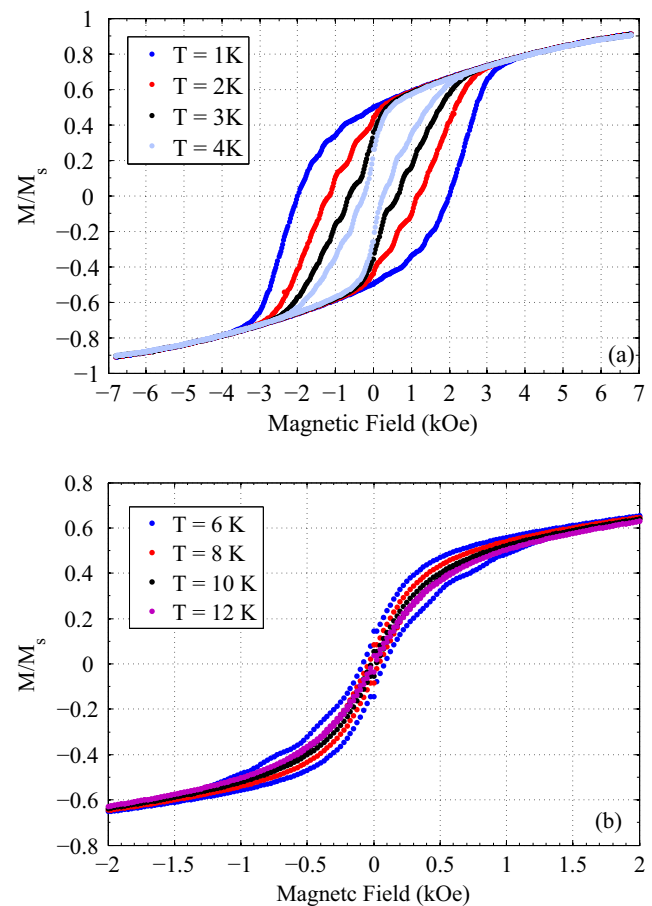


Fig. 5 The simulated hysteresis loop magnetization of Ni-ZnO nanoparticles. The nanoparticles moment transit from ferromagnetic to superparamagnetic, remanence goes toward zero, as the temperature exceeds $\langle T_B \rangle$

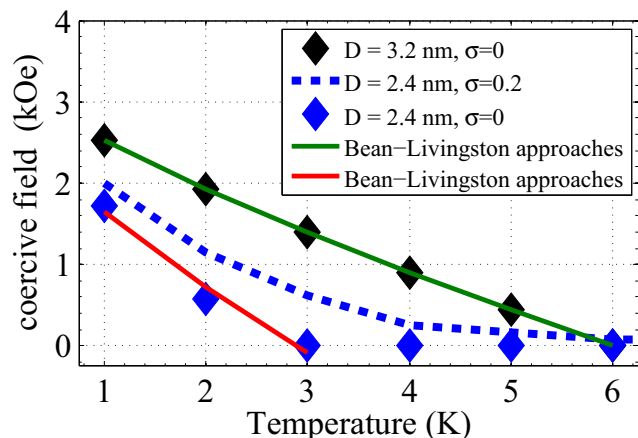


Fig. 6 The temperature dependencies of coercive field of Ni-ZnO nanoparticles for both single volume and non-uniform volume distribution. The results of coercive output are in good agreement with the theoretical Bean-Livingston approaches

is consequently expected. For $T > 10$ K, all nanoparticles in the sample behave superparamagnetically and the

hysteresis loop indicates that both the coercive field and remanence equal zero.

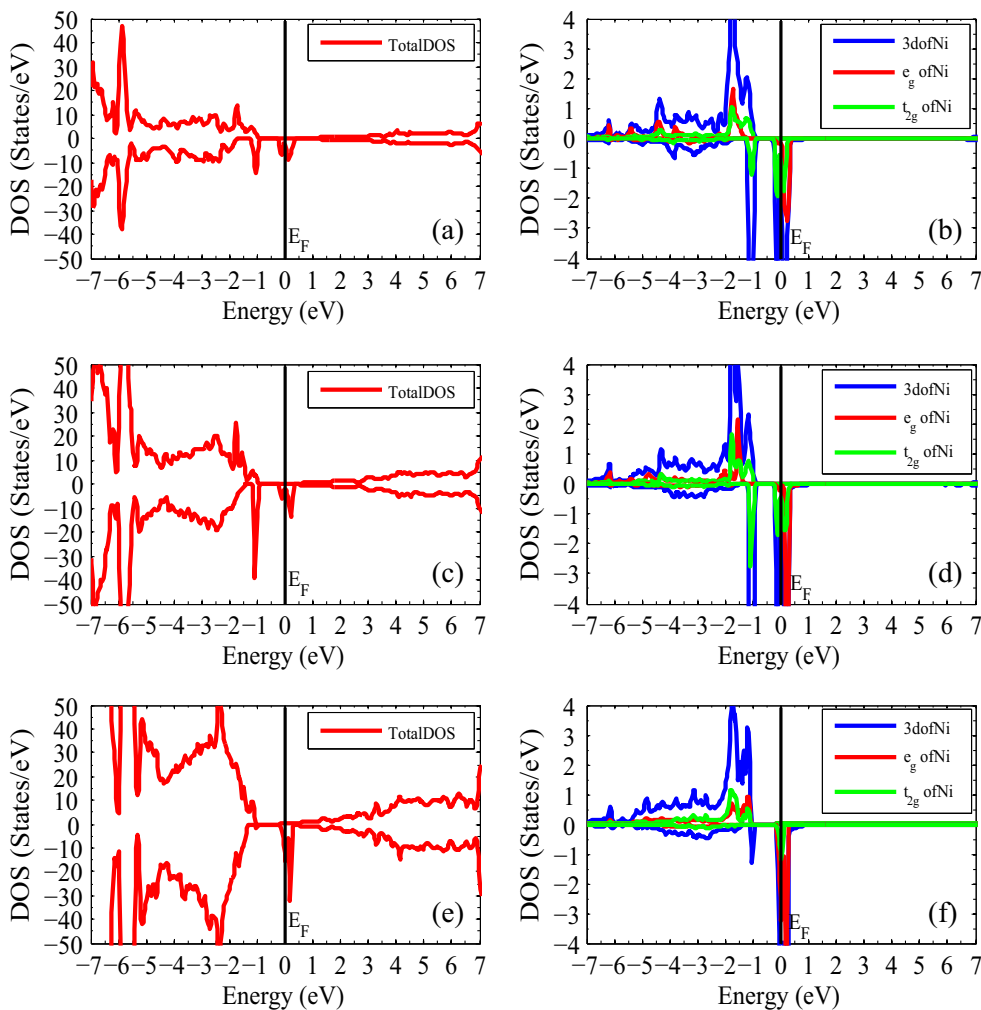
According to Fig. 5, as the temperature decreases, the coercive field begins to move toward higher strength magnetic fields. This was expected because the T_B was distributed primarily at about 1.8 K. Decreasing the temperature increased the number of particles entering the blocking state and behaving ferromagnetically.

Comparison of the coercive field for single-volume particles ($\sigma = 0$) and log-normal distributed particles ($\sigma = 0.2$) highlights the importance of non-uniform particle volume distribution (Fig. 6). For identical and non-interacting nanoparticles, the variation in coercive field for the blocked particles can be described using a formula based on Neel relaxation and the Bean-Livingston approach as [18, 35]:

$$H_c(T) = 0.48 \frac{2K}{M_s} \left[1 - \left(\frac{T}{T_B} \right)^{\frac{1}{2}} \right] \quad (12)$$

The temperature dependency of the coercive field of the single-volume nanoparticle is fitted to (12) for diameters of 2.4 and 3.2 nm. The simulated coercive field values

Fig. 7 The total DOS and partial DOS of $Zn_{1-x}Ni_xO$ compound for: **a, b** $x = 0.125$, **c, d** $x = 0.062$, and **e, f** $x = 0.028$



for single-volume clusters are in good agreement with the results of the Bean-Livingston approach. Moreover, as the particle volumes increased, the coercive field strength increased. The figure indicates that particle volume distribution with a median of 2.4 nm where $\sigma = 0.2$ produce greater coercive fields and superparamagnetism at higher temperatures.

3.2 Structural Properties

The structural and magnetic properties of $\text{Zn}_{1-x}\text{Ni}_x\text{O}$ compound ($x = 0.125, 0.062, \text{ and } 0.028$) using the first principle calculations is also investigated. The density of state (DOS) and partial DOS (PDOS) of the configurations are calculated and the results are shown in Fig. 7.

By submitting Ni into a cation site, because of the existence of strong hybridization between the 3d band of Ni and 2p band of O in the valance band, caused the 3d states of Ni atom to split into double degenerate e_g and triple degenerate t_{2g} states where the e_g levels have lower energies than the t_{2g} levels.

From Fig. 7b, d, f, it can be understood that the Ni 3d bands are fully occupied in the majority spin channel, and the minority spin channel of 3d levels energy band of Ni are partly occupied and cross the Fermi level, leading to the half metallic ferromagnetism behaviors. Because the DFT calculations were carried out at zero temperature, the magnetic behavior observed are in acceptable agreement with recently published experimental data [15] and confirm the results presented in Section 3.1

The equivalent total energy and the magnetic moment of three concentration of Ni-doped ZnO are shown in Table 2. The results indicate that the value of the total magnetic moment primarily corresponds to the Ni atom (more than 80 %) and the remaining contribution of the magnetic moment corresponds to the Zn and oxygen atoms. Increasing the concentration of Ni increases the hybridization between the 3d band of Ni and 2p band of its neighboring O atoms, which leads to reduction in the magnetic moment and energy gap. It can be concluded that the stability of the system closely relates to the Ni concentration; at higher concentrations, the total energy of the alloy increased, consequently leads to the reduction of the stability.

Table 2 The equivalent total energy, the magnetic moment of Ni atoms, and the total magnetic moment obtained by DFT calculation for different concentration of Ni in ZnO

Composition	E_{tot} (keV)	M_{Ni} (μ_B)	M_{tot} (μ_B)
$\text{Zn}_{0.875}\text{Ni}_{0.125}\text{O}$	-399.895	1.534	2.01
$\text{Zn}_{0.938}\text{Ni}_{0.062}\text{O}$	-807.283	1.546	2.02
$\text{Zn}_{0.972}\text{Ni}_{0.028}\text{O}$	-1825.752	1.564	2.06

4 Conclusion

A numerical model was used to simulate the FC/ZFC magnetization and the hysteresis loop of Ni-doped ZnO nanoparticles. This model was developed to account for the effect of the non-uniform distribution of the nanoparticles. The improvement led to acceptable agreement with the available experimental data for FC/ZFC magnetization. The results show that the average blocking temperature of about 1.8 K for Ni-doped ZnO nanoparticles is distributed over a log-normal distribution function with an average diameter of 2.4 nm and $\sigma = 0.2$. For temperatures above $\langle T_B \rangle$, nanoparticles transformed from a ferromagnetic state to a superparamagnetic state and, for $T > 10$ K, all nanoparticles transformed to the super-paramagnetic state. It was found that considering the distribution of nanoparticles for coercive field calculations causes deviation from the theoretical Bean-Livingston approach; however, the results for the single-volume nanoparticles agreed well with this theory.

The DFT method was employed to study the structural and electronic properties of $\text{Zn}_{1-x}\text{Ni}_x\text{O}$ ($x = 0.028, 0.062, \text{ and } 0.125$) nanoparticles. The results showed that increasing the Ni concentration decreases the values of the magnetic moment and energy gap of the compound and ferromagnetic behavior was observed for all concentrations. This magnetic behavior was in acceptable agreement with both the experimental data and the simulation results obtained in this work.

References

- Bouaoud, A., Rmili, A., Ouachtari, F., Louardi, A., Chtouki, T., Elidrissi, B., Erguig, H.: Transparent conducting properties of Ni doped zinc oxide thin films prepared by a facile spray pyrolysis technique using perfume atomizer. *Mater. Chem. Phys.* **137**, 843e847 (2013)
- Gal, D., Hodes, G., Lincot, D., Schock, H.-W.: Electrochemical deposition of zinc oxide films from non-aqueous solution: a new buffer/window process for thin film solar cells. *Thin Solid Films* **361**, 79e83 (2000)
- Haga, K., Katahira, F., Watanabe, H.: *Thin Solid Films* **343**, 145e147 (1999)
- Roy, S., Basu, S.: Improved zinc oxide film for gas sensor applications. *Bull. Mater. Sci.* **25**(6), 513e515 (2002)
- Dietl, T., Ohno, H.: Dilute ferromagnetic semiconductors: Physics and spintronic structures. *Rev. Mod. Phys.* **86**, 187 (2014)
- Yang, Z.: A perspective of recent progress in ZnO diluted magnetic semiconductors. *Appl. Phys. A* **112**, 241e254 (2013)
- Dietl, T.: A ten-year perspective on dilute magnetic semiconductors and oxides. *Nat. Mater.* **9**, 965–974 (2010)
- Dietl, T., Ohno, H., Matsukura, F., Cibert, J., Ferrand, D.: Zener model description of ferromagnetism in zinc-blende magnetic semiconductors. *Science* **287**, 1019–1022 (2000)
- Margarethe, H.-A. et al.: Nanostructured materials for biomedical applications, p119–149. Kerala, India (2009)

10. Rotello, V.M.: Nanoparticles: building blocks for nanotechnology Springer Science & Business Media (2004)
11. Schmid, G.: Nanoparticles from theory to application, pp. 271–281. Wiley-VCH Verlag GmbH & Co. KGaA, Weinheim (2010)
12. Cai, X., Cai, Y., Liu, Y., Li, H., Zhang, F., Wang, Y.: Structural and photocatalytic properties of nickel-doped zinc oxide powders with variable dopant contents. *J. Phys. Chem. Solids* **74**, 11961203 (2013)
13. Kant, S., Pathania, D., Singh, P., Dhiman, P., Kumar, A.: Removal of malachite green and methylene blue by Fe 0.01 Ni 0.01 Zn 0.98 O/polyacrylamide nanocomposite using coupled adsorption and photocatalysis. *Appl. Catal. Environ.* **147**, 340–352 (2014)
14. Shayesteh, S.F., Nosrati, R.: The Structural and Magnetic Properties of Diluted Magnetic Semiconductor Zn_{1-x}Ni_xO Nanoparticles. *J. Supercond. Nov. Magn.* **28**, 18211826 (2015)
15. Borges, R.P., Ribeiro, B., Cruz, M.M., Godinho, M., Wahl, U., da Silva, R.C., Gonçalves, A.P., Magén, C.: Nanoparticles of Ni in ZnO single crystal matrix. *Eur. Phys. J. B* **17**, 86 (2013)
16. Das, S.C., Green, R.J., Podder, J., Regier, T.Z., Chang, G.S., Moewes, A.: Band gap tuning in ZnO through Ni doping via spray pyrolysis. *J. Phys. Chem. C* **117**, 1274512753 (2013)
17. Chiu, S.H., Hsu, H.S., Huang, J.C.A.: Magneto-Optical Properties of Ni ZnO Nanorods. *IEEE Trans. Magn.* **48**, 3933–3935 (2012)
18. Tamion, A., Bonet, E., Tournus, F., Raufast, C., Hillion, A., Gaier, O., Dupuis, V.: Efficient hysteresis loop simulations of nanoparticle assemblies beyond the uniaxial anisotropy. *Phys. Rev. B* **85**, 134430 (2012)
19. Usov, N.A., Grebenshchikov, Y.B.: Hysteresis loops of an assembly of superparamagnetic nanoparticles with uniaxial anisotropy. *J. Appl. Phys.* **106**, 023917 (2009)
20. Fang, W.X., He, Z.H., Chen, D.H., Shao, Y.Z.: The effect of randomly oriented anisotropy on the zero-field-cooled magnetization of a non-interacting magnetic nanoparticle assembly. *J. Magn. Magn. Mater.* **321**, 4032–4038 (2009)
21. Gu, G., Xiang, G., Luo, J., Ren, H., Lan, M., He, D., Zhang, X.: Magnetism in transition-metal-doped ZnO: a first-principles study. *J. Appl. Phys.* **112**, 023913 (2012)
22. Chien, C.-H., Chiou, S.H., Guo, G., Yao, Y.-D.: Electronic structure and magnetic moments of 3d transition metal-doped ZnO. *J. Magn. Magn. Mater.* **282**, 275–278 (2004)
23. Elilarassi, R., Chandrasekaran, G.: Synthesis, structural and optical characterization of Ni-doped ZnO nanoparticles. *J. Mater. Sci. Mater. Electron.* **22**, 751–756 (2011)
24. Xu, X., Cao, C.: Hydrothermal synthesis and magneto-optical properties of Ni-doped ZnO hexagonal columns. *J. Magn. Magn. Mater.* **377**, 308–313 (2015)
25. Luis, F., Torres, J.M., García, L.M., Bartolomé, J., Stankiewicz, J., Petroff, F., Fetta, F., Maurice, J.-L., Vaures, A.: Enhancement of the magnetic anisotropy of nanometer-sized Co clusters Influence of the surface and of interparticle interactions. *Phys. Rev. B* **094409**, 65 (2002)
26. Usov, N.A.: Numerical simulation of field-cooled and zero field-cooled processes for assembly of superparamagnetic nanoparticles with uniaxial anisotropy. *J. Appl. Phys.* **109**, 023913 (2011)
27. Chantrell, R.W., Walmsley, N., Gore, J., Maylin, M.: Calculations of the susceptibility of interacting superparamagnetic particles. *Phys. Rev. B* **024410**, 63 (2000)
28. Blaha, P., Schwarz, K., Madsen, G.K.H., Kvasnicka, D., Luitz, J.: WIEN 2K, An Augmented Plane Wave + Local Orbitals Program for Calculating Crystal Properties, ISBN 3-9501031-1-2. Karlheinz Schwarz, Techn. Universitt Wien, Austria (2001)
29. Madsen, G.K.H., Blaha, P., Schwarz, K., Sjustedt, E., Nordström, L.: Efficient linearization of the augmented plane-wave method. *Phys. Rev. B* **64**, 195134 (2001)
30. Perdew, J.P., Burke, K., Ernzerhof, M.: Generalized gradient approximation made simple. *Phys. Rev. Lett.* **77**, 3865 (1996)
31. Pal, B., Sarkar, D., Giri, P.K.: Structural, optical, and magnetic properties of Ni doped ZnO nanoparticles: Correlation of magnetic moment with defect density. *Appl. Surf. Sci.* **356**, 804–811 (2015)
32. Decremps, F., Datchi, F., Saitta, A.M., Polian, A., Pascarelli, S., Di Cicco, A., Itié, J.P., Baudelet, F.: Local structure of condensed zinc oxide. *Phys. Rev. B* **68**, 104101 (2003)
33. Knobel, M., Nunes, W.C., Socolovsky, L.M., De Biasi, E., Vargas, J.M., Denardin, J.C.: Superparamagnetism and other magnetic features in granular materials: a review on ideal and real systems. *J. Nanosci. Nanotechnol.* **8**, 2836–2857 (2008)
34. Denardin, J.C., Brandl, A.L., Knobel, M., Panissod, P., Pakhomov, A.B., Liu, H., Zhang, X.X.: Thermoremanence and zero-field-cooled/field-cooled magnetization study of Co x (SiO 2) 1- x granular films. *Phys. Rev. B* **65**, 064422 (2002)
35. Nunes, W.C., Folly, W.S.D., Sinnecker, J.P., Novak, M.A.: Temperature dependence of the coercive field in single-domain particle systems. *Phys. Rev. B* **70**, 014419 (2004)